

# Research on Precise Retrieval Methods for Three-Dimensional Bushing Components Using SolidWorks Sketch Profile Features

Xin Shao<sup>1</sup>, Yawen Fan<sup>2,\*</sup>, Jingfeng Shen<sup>1,\*</sup>, LiangWei Zhong<sup>1</sup>

<sup>1</sup>*School of Mechanical Engineering, University of Shanghai for Science and Technology, Shanghai, China*

<sup>2</sup>*School of Engineering and Computing, University of Shanghai for Science and Technology, Shanghai, China*

*\*Corresponding Author*

**Abstract:** To facilitate efficient reuse of bushing components in mechanical design, an accurate 3D retrieval method based on SolidWorks sketch profile features is proposed to overcome limitations of existing approaches, including inadequate capture of local design features, dependence on sketch or view data, and poor format compatibility. The proposed method extracts the core sketch for rotationally formed bushing parts via the SolidWorks API and represents it as an ordered sequence of line segments obtained through sketch decomposition. A feature descriptor is constructed using a five-tuple consisting of length, direction angle, line segment type, diameter, and keyway type. Based on this representation, a main contour matching strategy that integrates bidirectional angle mapping with sliding-window matching is employed to evaluate the contour sequence similarity between the query sketch and candidate models in the part library. A special scenario verification mechanism is further introduced to refine the similarity score, supplemented by engineering correction rules that enforce consistency in keyway configuration and outer diameter. The final output is a normalized similarity value within the range of [0, 1]. Experimental validation was conducted on an initial dataset of 500 industrial-grade bushing parts, from which 466 valid models were retained after data screening. The proposed method was evaluated in comparison with CADFind3D, a mainstream industrial CAD retrieval tool based on global shape features. When the top 10 ranked retrieval results were considered for performance evaluation, the proposed five-tuple feature retrieval method based on SolidWorks sketch profiles achieved a precision of 84.5%, a recall of 78.67%, an F1-

score of 80.97%, and a mean average precision (MAP) of 87.99%, representing improvements of 172.5%, 174.4%, 177.6%, and 259.88%, respectively, over CADFind3D. These results demonstrate that the proposed method can effectively capture fine-grained design differences, such as local groove types and shaft-section transitions, thereby providing robust technical support for design intent-driven part reuse.

**Keywords:** Bushing Parts; SolidWorks Sketch Profile; Five-Tuple Feature Description; Bidirectional Angle Mapping; Sliding Window Matching; 3D Model Retrieval

## 1. Introduction

Efficient reuse of mechanical part designs is essential for improving R&D productivity and reducing production costs in modern manufacturing environments characterized by rapid product iteration [1]. 3D model retrieval technology serves as a key enabler for part reuse, and in recent years, relevant research has formed a development pattern featuring the parallel advancement of multiple technical routes.

From the perspective of data input formats, there are end-to-end retrieval solutions based on sketches. For instance, the triple hierarchical metric network method proposed by Yang Zhanyan et al. can effectively improve the retrieval performance of the network [2]. There are also retrieval algorithms relying on view information, such as the internal-external view fusion model developed by Zhou Yan's team and the single-view attention retrieval method proposed by Han Xiaofan et al. These approaches can achieve universal retrieval and classification of 3D models through 2D view feature mapping [3,4]. However, these two types

of retrieval methods either depend on sketch drawing input or require multi-view image acquisition, which increases the operational burden on designers.

In terms of feature extraction and matching technologies, deep learning methods have demonstrated strong feature learning capabilities. Zhu Tong developed 3D mechanical part retrieval technology and corresponding software based on the PointNet neural network [5]. Ji Hao conducted research on 3D medical rehabilitation aids, proposing and exploring a classification and retrieval method for such aids based on point cloud features [6]. Cheng Pu constructed the GNMR method using graph neural networks to achieve accurate retrieval of 3D neuron geometric shapes [7]. Nevertheless, these general deep learning retrieval models take point cloud data as their core processing object. They require converting bushing parts in SolidWorks' SLDprt format into point clouds first, and this data conversion process is prone to damaging the parametric constraints and topological relationships of the bushing parts. Meanwhile, their training relies on large-scale annotated datasets, making it difficult to directly integrate them into lightweight industrial-grade mechanical design workflows.

Among traditional methods, the 3D tire pattern retrieval scheme based on geometric features proposed by Fan Hongyu et al. has also verified the retrieval advantages of domain-specific geometric features in specific scenarios [8]. However, this method exhibits weak ability in identifying local features, and the complex geometric feature matching process incurs certain computational costs, resulting in insufficient real-time performance.

Furthermore, in the extended field of 3D retrieval technology, Tai Tianyang proposed video retrieval technology based on 3D convolutional neural networks [9]. This technology achieves accurate video content retrieval by leveraging the ability of 3D convolution to deeply mine spatiotemporal dimension features. This feature extraction idea can provide technical reference for the multimodal fusion-based bushing part retrieval system. Nevertheless, there is an adaptability gap between its model architecture designed for video temporal data and the retrieval requirements of static 3D models of mechanical parts, preventing direct migration and application.

This study takes guide bushing components as the research object, focusing on issues in 3D retrieval such as reliance on sketch or view data and format incompatibility, and conducts in-depth exploration of 3D retrieval methods suitable for SLDprt files. By constructing an algorithm that identifies the shape of SLDprt files and judges similarity, experiments on 3D retrieval of guide bushing are carried out.

Based on this, this paper proposes a feature encoding method for bushing parts based on SolidWorks sketch profiles to accurately capture local structural details. A sliding window matching algorithm is adopted to adapt to the length differences and local misalignments of bushing contour sequences, thereby improving the accuracy of similarity calculation. The effectiveness of the method is verified using an industrial-grade dataset, providing an engineering solution for the efficient reuse of bushing parts. This method realizes automatic sketch extraction and preprocessing based on the SolidWorks API, eliminating the need for model format conversion and enabling direct integration with industrial design workflows.

## 2. Design of Five-Tuple Feature Retrieval Algorithm Based on SolidWorks Sketch Profile

### 2.1 Research Object

The research object of this study is bushing components, with guide bushing as a typical representative. All parts in the model library used for algorithm verification are hydraulic cylinder guide bushing. A hydraulic cylinder guide sleeve is a sleeve-type cylinder part that guides and supports the piston rod. Generally, sealing grooves are designed and machined on both the inner and outer cylindrical surfaces, which are used for the static sealing of the piston, the dynamic sealing of the piston rod, and the dust prevention of the piston rod. The guide bushing involved in this study are mainly divided into two categories: Type A and Type B. Type A guide bushing are equipped with 2 seal grooves and a multi-layer stepped protrusion structure, presenting an overall "gradually shrinking" profile. In contrast, Type B guide bushing have only 1 seal groove, with fewer changes in stepped protrusions, and both the left and right sides show large-area smooth surfaces, as illustrated in Figure 1.

Beyond the structural differences outlined above,

guide bushing also feature keyways, which are categorized into three core configurations: keyless (Type I), square keyway (Type II), and circular hole (Type III). The keyway types are illustrated in Figure 2.



**Figure 1. Classification of Guide Bushing**



**Figure 2. Classification of Keyways**

The core functional differences of guide bushing are determined by local detailed features; however, existing 3D retrieval technologies struggle to effectively capture these critical differences, as elaborated below:

**Structural Details Perspective:** Local features of guide bushing directly affect assembly performance. For instance, both square keyways and circular-hole keyways are used for torque transmission, but the former is adapted for flat key connections, while the latter is suitable for semicircular key connections. Failure to

distinguish such differences during retrieval may lead to assembly failure.

**Dimensional Accuracy Perspective:** Minor dimensional differences in guide bushing—such as step height differences and seal groove widths—exert a significant impact on the positioning accuracy of the shaft system and sealing performance. Nevertheless, traditional retrieval methods primarily focus on overall shape similarity, easily overlooking these local dimensional variations. This oversight results in retrieval outcomes that appear similar in form but differ substantially in actual functionality.

**3D Modeling Data Feature Perspective:** Since guide bushing are rotational parts, the method of rotational forming via cross-sectional profile sketches is highly appropriate. A cross-sectional profile sketch contains all the geometric information of the part and serves as the core sketch (as shown in Figure 3). It acts as a key data carrier for the accurate representation of design intent and retrieval. In addition, there are auxiliary sketches, which are specialized sketches drawn during the SolidWorks modeling of bushing parts to construct local functional features. Their core role is to assist in the generation of keyways.

Therefore, taking the SolidWorks sketch profile of bushing parts as the entry point not only avoids feature loss caused by model format conversion but also directly aligns with the original data logic of engineering design, laying a foundation for the accurate retrieval and reuse of parts.

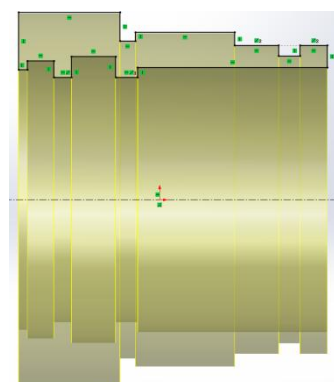


**Figure 3. SolidWorks Sketch Profile of the Guide Sleeve**

## 2.2 Overall Framework of the Method

This study further subdivides the workflow of the 3D model sketch retrieval task into three phases: the preprocessing phase, the database construction phase, and the retrieval phase. The overall framework is illustrated in Figure 4.

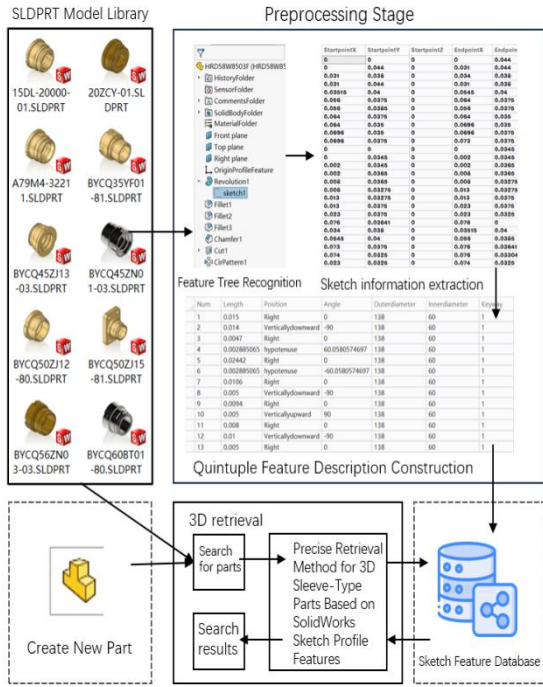


**Figure 4. Framework of the SolidWorks Sketch Profile Feature Recognition Method**

Preprocessing Phase: Through the SolidWorks API, feature tree recognition is performed on 3D models to extract sketches.

Database Construction Phase: Algorithms are used to identify sketch features, standardize these features, and store them in the database [10, 11].

Retrieval Phase: Files are opened via SolidWorks, which can be either library files or newly created SLDprt files. Algorithms identify the features of these files and match them with data in the database to obtain similarity results between the currently opened part and all other parts in the library. The results are sorted, and finally, the top results with the highest similarity are output.

### 2.3 Sketch Information Extraction and Construction of Five-Tuple Feature Description

#### 2.3.1 Sketch screening and information extraction

The sketches of bushing parts consist of "core sketches" and "auxiliary sketches". Therefore, core sketches must be screened according to the following rules:

Rule 1: A core sketch must be associated with a rotational feature.

Rule 2: A core sketch must be a closed contour.

Rule 3: A core sketch must contain no fewer than 4 line segments.

By clearly distinguishing between core sketches

and auxiliary sketches, hierarchical feature extraction of "overall shape + local structure" for bushing parts can be achieved, laying a clear data foundation for the subsequent construction of the five-tuple feature description.

#### 2.3.2 Construction of five-tuple feature description

A screened core sketch is essentially an ordered contour composed of several line segments. The extracted information includes the endpoint coordinates of each line segment in the sketch. To realize the quantitative description of the geometric features of the core sketch, these endpoint coordinates need to be converted into "line segment feature entities" that enable shape recognition, so as to obtain the attribute information of the line segments [12]. In addition, the information of auxiliary sketches must be identified to acquire keyway features. Based on the information obtained from the two types of sketch recognition, the core dimensions of line segment feature entities can be designed as a five-tuple feature description, with each attribute of the five-tuple specified as follows:

a) Length Attribute: Refers to the actual geometric length of the line segment, which serves as the basis for characterizing the structural dimensions of the part.

b) Angle Attribute: Includes the original angle and the mapped angle. The original angle is the actual angle of the line segment in the 3D coordinate system, while the mapped angle is used to handle matching in scenarios where the contour direction is mirrored.

c) Direction Attribute: Determines whether a line segment is horizontal or vertical through angle thresholds, with the following judgment rules:

i. Horizontal line segments: The absolute value of the mapped angle is close to  $0^\circ$  or  $180^\circ$ .

ii. Vertical line segments: The absolute value of the mapped angle is close to  $90^\circ$ , where positive values indicate an upward direction and negative values indicate a downward direction.

iii. Oblique lines (as shown in Figure 5): Line segments that are neither horizontal nor vertical, with positive/negative values indicating directions consistent with those of vertical line segments.

iv. Arcs (as shown in Figure 6): Generally correspond to fillet features, which are classified as micro-features and will be filtered out in the algorithm.

d). Diameter Attribute: Defined as the maximum

step diameter of the bushing model.

e). Keyway Attribute: Refers to the type of keyway on the part.

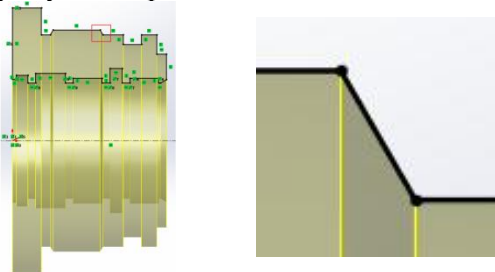


**Figure 5. Schematic Diagram of Oblique Line Sketches**

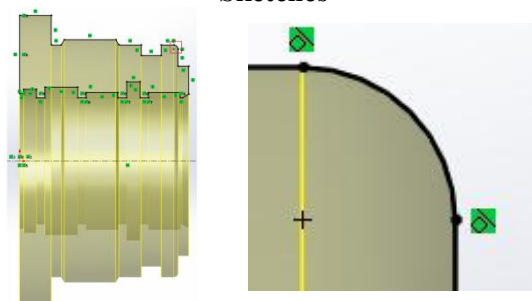


**Figure 6. Schematic Diagram of Arc Sketches**

### 2.3.3 Micro-feature processing

After obtaining the five-tuple descriptions of all "line segment feature entities", additional processing of micro-features is required. This is because numerous micro-features interfere with the overall shape and affect subsequent similarity calculations. The specific process is as follows:

(1) Extraction of Valid Line Segments: The original contour data may contain invalid line segments with lengths approaching 0. Such invalid data must be filtered out first to ensure feature validity. The rule for extracting valid line segments is as follows: traverse the input line segment data table, filter out line segments with lengths greater than a minimal threshold, convert them into standardized line segment feature entities, and form valid line segment sequences  $seqA/seqB$ [13].

(2) Filtering of Main Contour Line Segments: A large number of micro-feature line segments exist in the contours of bushing parts. These features are susceptible to machining errors and measurement accuracy, and their contribution to the overall structural similarity of parts is extremely low. To focus on core structural features, this study introduces a micro-feature

threshold (2 mm by default) to filter out micro-line segments and extract main contour line segments. The core formula is:

$$L_{min} = \bar{L} \times r_{min} \quad (1)$$

Where:  $\bar{L}$  is the average length of the valid line segment sequence;  $r_{min}$  is the micro-feature threshold;  $L_{min}$  is the minimum length threshold for main contour line segments.

(3) Processing of Chamfer and Fillet Details: Arc features such as chamfers and fillets of bushing parts belong to structural details. Although they are significant for part machining processes and assembly performance, their core contribution to the overall contour structural similarity is low. Moreover, such arcs are easily confused with micro-line segments and thus require differentiated processing based on data features.

In the original contour data: The beveled edge features of chamfers are filtered using the micro-feature threshold; the arc features of fillets are marked with Size = 0 (distinguished from straight line segments with Size = 1). These two types of features do not possess independent main contour attributes and need to be attached to adjacent valid straight line segments for dimension integration, rather than being extracted as independent main contour line segments.

The beveled edges of chamfers and the arcs of fillets do not generate independent main contour line segment records, which avoids the interference of micro-arc features on the extraction and analysis of core contours. However, their dimensional contributions are retained: the arc radius values or the sine/cosine values of the beveled edges are integrated into the lengths of adjacent valid straight line segments. This ensures the integrity of the overall contour dimensions without damaging the continuity of the main contour line segments. Through this processing method, two objectives are achieved simultaneously:

It filters out the interference of non-core details (such as chamfers/fillets) on main contour analysis, focusing on the core structural features of bushing parts;

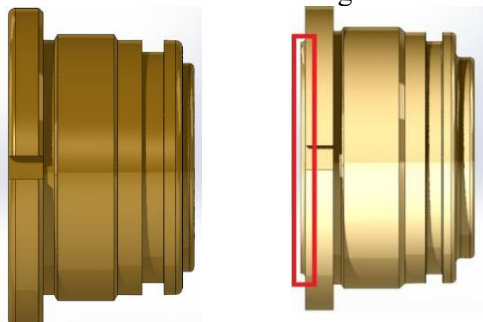
It retains the actual dimensional contributions of arcs through dimension integration, avoiding the distortion of overall contour dimensions caused by filtering micro-features.

This balances the simplicity of main contour extraction and the integrity of dimensional data.

## 2.4 Similarity Retrieval Algorithm

### 2.4.1 Main contour matching

Main contour matching is the core link of similarity calculation, whose goal is to achieve accurate alignment of two groups of main contour line segments so as to quantify the degree of feature matching. This study designs a strategy combining bidirectional angle mapping and sliding window matching to optimize the matching start range [14,15]. Meanwhile, scenarios involving micro-protrusions and micro-grooves are distinguished. A schematic diagram of micro-protrusions is shown in Figure 7. Compared with the original part, the part with an extra protrusion has an additional micro-step protrusion. Such local micro-protrusions have limited impact on the core features of the overall contour structure but will increase the number of main contour line segments by 1-3. If such scenarios are not distinguished specifically, it is easy to misjudge the structural similarity due to the difference in the number of line segments during the matching process, and the same applies to the features of micro-grooves.



(a) Part without an Extra Protrusion      (b) Part with an Extra Protrusion  
**Figure 7. Schematic Diagram of Micro-Protrusions**

### (1) Reverse angle mapping mechanism

The 3D models of bushing parts may exhibit contour direction mirroring (e.g., left-right flipping). Directly using the original angle for matching will lead to missed matches of valid contours. To address this, reverse angle mapping rules are designed as follows:

**Vertical line segments:** The mapped angle remains consistent with the original angle, as the direction of vertical line segments is insensitive to mirroring.

**Non-vertical line segments:** The mapped angle is calculated as  $180^\circ - \text{OriginalAngle}$ , and the result is normalized to the range of  $0\text{--}180^\circ$  to adapt to the angle matching requirements of mirrored contours.

During the matching process, matching is performed for three scenarios: original angles, reversed angles of Group A, and reversed angles of Group B. The optimal matching result is selected to ensure that differences in contour directions do not affect the matching accuracy.

### (2) Sliding Window Matching Strategy

To find the most comparable part between two sequences, this study adopts a constrained sliding window matching algorithm. The algorithm aims to find the starting indices ( $i_{s,j_s}$ ) such that the length  $L$  of continuous matching starting from this position is maximized. The matching process must satisfy the following two core constraints:

**Angle consistency constraint:** The direction categories of the feature units at corresponding positions must be consistent.

$$\text{Match}_\theta(U_{A,k}, U_{B,k}) = \begin{cases} \text{True,} & \text{if } (r_{A,k} = r_{B,k} = H) \text{ or} \\ & (r_{A,k} = r_{B,k} = V \text{ and } \theta_{A,k} = \theta_{B,k}) \\ & (r_{A,k}, r_{B,k} \notin \{H, V\} \text{ and } \theta_A = \theta_B) \\ \text{False,} & \text{otherwise} \end{cases} \quad (2)$$

Where:  $\text{Match}_\theta$  represents the "angle matching judgment function";  $U_{A,k}$  and  $U_{B,k}$  respectively denote the line segment feature units of Group A and Group B at the  $k$ -th position in the sliding window;  $r_{A,k}$  and  $r_{B,k}$  are the direction category identifiers of the corresponding feature units;  $H$ ,  $V$ ,  $\theta_{A,k}$ ,  $\theta_{B,k}$  are the direction attributes in the five-tuple feature description.

**Proportion Benchmark Constraint:** During matching, the length ratio of the first 3 pairs of matched line segments is used as the local proportion benchmark  $R_b$  for normalizing subsequent length comparisons to eliminate the impact of overall scaling.

$$R_b = \frac{\sum_{k=0}^2 l_{A,i_s+k}}{\sum_{k=0}^2 l_{B,j_s+k}} \quad (3)$$

The algorithm traverses all possible starting positions of  $S_A^m$  and  $S_B^m$  through double loops to find the longest continuous matching subsequence that satisfies the above constraints. To handle potential opposite contour drawing directions, the algorithm also performs reverse angle mapping on sequences  $S_A^m$  and  $S_B^m$ , and executes matching in three combinations: original sequence, reversed Group A, and reversed Group B. The result with the longest matching length is selected as the optimal match  $R_{best}$ .

$$\theta' = \begin{cases} \theta, & \text{if } r=V \\ 180-\theta, & \text{if } r \neq V \end{cases} \quad (4)$$

#### 2.4.2 Multi-dimensional weighted similarity scoring mechanism

After the main contour matching is completed, the similarity score is calculated from four core dimensions based on the matching results, and coefficients are assigned according to the weight of each dimension on the structural similarity of bushing parts. The core formula is:

$$S_{\text{base}} = S_{\text{angle}} \times w_{\theta} + S_{\text{horizontal}} \times w_h + S_{\text{vertical}} \times w_v + S \quad (5)$$

Where:  $w_{\theta}=0.55$ ,  $w_h=0.35$ ,  $w_v=0.05$ ,  $w_r=0.05$ .

Based on the optimal matching result  $R_{best}$ , the similarity score is calculated from four dimensions:

(1) Angle matching rate  $S_{\theta}$  : Evaluates the consistency of contour trends.

$$S_{\theta} = \frac{C\theta}{\max(m,n)} \times w_{\theta} \quad (6)$$

Where:  $C\theta$  is the number of units with consistent angles in the matching units.

(2) Horizontal length similarity  $S_h$  : Compares the total length of all horizontal line segments. Let the total horizontal length of Group A in the matching segment be  $L_{hA}$ , and the total horizontal length of Group B after scaling by the proportion benchmark be  $L_{hB}$ .  $R_b$ .

$$E_h = \frac{|L_{hA} - L_{hB} \cdot R_b|}{\max(L_{hA}, L_{hB} \cdot R_b)} \quad (7)$$

$$S_h = (1 - \min(E_h, 1)) \times w_h \quad (8)$$

(3) Vertical length similarity  $S_v$  compares the lengths of vertical line segments pair by pair. For the  $k$ -th pair of vertical units, the error is calculated as  $e_v^k = |l_{A,k} - l_{B,k} \cdot R_b| / l_{A,k}$ . If  $e_v^k$  is less than the tolerance  $\tau$  (default 0.15), its similarity is  $1 - e_v^k$ ; otherwise, it is 0.  $S_v$  is the average value multiplied by the weight.

$$S_v = \left( \frac{1}{N_v} \sum_{k=1}^{N_v} I(e_v^k \leq \tau) \cdot (1 - e_v^k) \right) \times w_v \quad (9)$$

Where:  $N_v$  is the number of pairs of matched vertical line segments;  $I$  is the indicator function.

(4) Proportion deviation score  $S_r$  : Penalizes overall proportion differences.

$$S_r = (1 - \min(|R_b - 1|, 0.5)) \times w_r \quad (10)$$

#### 2.4.3 Scenario-Specific deduction and proportion consistency verification

To accurately reflect structural differences, the algorithm introduces deduction items based on matching analysis and scenario discrimination.

##### (1) Protrusion/Groove Scenario Deduction

The structural differences of bushing parts are mainly reflected in two scenarios: protrusions and grooves. Basic deduction ( $D_{\text{base}}$ ) rules need

to be designed for different scenarios:

Groove scenario deduction: Calculate the ratio of the total "projection difference"  $\Delta P$  of matched vertical line segments in the vertical direction to the total length  $L_{\text{total}}$  of the two contours, and perform mild to moderate deduction (0.01~0.1) according to the ratio.

Protrusion scenario deduction: Calculate the ratio  $R_{\text{boss}}$  of the total length of the "protrusion" part not involved in matching to the length of the main contour, and the deduction value increases with the increase of the ratio (0.05~0.2).

$$D_{\text{base}} = \begin{cases} f_{\text{pit}} \left( \frac{\Delta P}{L_{\text{total}}} \right), & \text{if groove scenario} \\ 0.05 + 0.15 \times R_{\text{boss}}, & \text{if protrusion scenario} \\ 0, & \text{otherwise} \end{cases} \quad (11)$$

Where:  $f_{\text{pit}}$  is a function that outputs the corresponding deduction coefficient based on the value of  $\frac{\Delta P}{L_{\text{total}}}$ .

##### (2) Length Proportion Consistency Verification

To solve the problem of similarity misjudgment caused by large proportion differences of key line segments, this study adds a length proportion consistency deduction ( $D_{\text{ratio}}$ ) mechanism. The core idea is: calculate the proportion difference (proportion of Group A - proportion of Group B) of each line segment in the matching interval to the total length in the corresponding direction (horizontal/vertical). Deduction rules are designed based on the number and distribution characteristics of differences exceeding the threshold ( $\text{ratio}_{\text{diffThreshold}}$ , default 0.05). To avoid misjudgment where the overall length is similar but the proportion of key parts is imbalanced, for each pair of matched horizontal/vertical line segments, calculate the proportion difference  $d_k = \text{ratio}_{A,k} - \text{ratio}_{B,k}$  of the segment in the cumulative length of its respective sequence.

If all  $|d_k| \leq \delta$  (threshold, default 0.05), then  $D_{\text{ratio}} = 0$ .

If only one difference exceeds the threshold, then  $D_{\text{ratio}} = \min(|d_k|, 0.1)$ .

If multiple differences exceed the threshold and all  $d_k$  have the same sign (regular mutation), then  $D_{\text{ratio}} = \min(0.5 \times \sum |d_k|, 0.3)$ ; if the signs are mixed (irregular structural differences), a direct deduction of  $D_{\text{ratio}} = 0.5$  is applied.

#### 2.4.4 Similarity correction and normalization

The comprehensive similarity  $Sim_{\text{raw}}$  is the sum of scores from each dimension minus the total deduction value, and is restricted to the range [0,

1]:

$$Sim_{raw} = \max[0, \min[1, S_\theta + S_h + S_v + S_r - (D_{base} + D_r)] \quad (12)$$

Finally, two engineering correction rules are applied:

(1) High Similarity Reward: If  $S_\theta = 1$ ,  $S_h \geq 0.9$  and the number of proportion differences exceeding the threshold is  $\leq 1$ , then  $Sim = \max[0, (Sim_{raw}, 0.85)]$ ; if  $S_h \geq 0.95$  and there are no proportion differences at the same time, then  $Sim = \max[0, (Sim_{raw}, 0.95)]$ .

(2) Key Attribute Penalty: If the keyway types of the two parts are different, then  $Sim = Sim - 0.05$ ; if the outer diameters are inconsistent, additional deduction is performed based on the error magnitude, specifically:  $Sim = Sim - Sim_{Radiuserror}$ . The final output value  $Sim \in [0, 1]$  is the similarity of the two rotational parts, with a higher value indicating a more similar contour.

### 3. Verification and Performance Analysis of the Five-Tuple Feature Retrieval Algorithm

#### 3.1 Data and Environment for Algorithm Verification

##### 3.1.1 Verification dataset

The experimental data is sourced from the bushing part library of a heavy machinery enterprise. The original part library contains 500 parts, and after data screening, 466 valid bushing parts are obtained. The research focuses on 20 typical query parts, all of which are in SolidWorks SLDprt format.

**Selection of Query Samples:** From 466 samples with "number of similar parts  $\geq 5$ ", 20 query parts are selected using stratified random sampling. The number of valid reference similar documents for these 20 query parts ranges from 8 to 21, with a median of 9.

**Details of Query Samples:** The list of query parts and the number of their reference similar parts are as follows: 15DL-20000-01 (10 parts), BYCQ63XF01-81 (9 parts), BYCX56BT01-80 (15 parts), BYCX70XF01-81 (21 parts), BYCX70YF01-80 (12 parts), BYGH50HW03-83DG (14 parts), BYGK50TK03-83 (10 parts), BYGK80TZ01-80 (19 parts), D69K8402-02 (12 parts), DH2S8-82031PJ (8 parts), G0YR4-32801L (8 parts), GCQ045XS-01 (8 parts), GCQ063BYT5-01 (9 parts), GCX063HW16-01 (16 parts), HRD58W8503F (9 parts), Q070DJ3-02 (15 parts), R0G28-81901-01 (12 parts), R0G28-82911 (9 parts), R2HU8-82801 (8 parts),

and T1HC7-62401 (8 parts).

##### 3.1.2 Verification environment

To ensure fairness, all methods are run in the same hardware and software environment. The specific configurations are shown in Table 1.

**Table 1. Environment Configuration**

Environment Type	Specific Configuration
Hardware Configuration	CPU: Intel Core i7-10400F (2.9GHz, maximum turbo frequency 4.3GHz); Memory: 32GB DDR5 2666MHz; Graphics Card: NVIDIA RTX 4060 (8GB video memory); Storage: 512GB NVMe SSD (system disk), 2TB SATA mechanical hard disk (data disk)
Software Environment	Operating System: Windows 11 Professional (21H2); 3D Software: SolidWorks 2022 SP5; Retrieval Tool: CADFind3D V4.2; Development Tool: VB.NET 8.0

#### 3.2 Algorithm Verification

##### 3.2.1 Selection of comparison method

CADFind3D V4.2, a commonly used SolidWorks retrieval plug-in in industry, is selected as the comparison method. This method is based on model surface topological feature matching and is widely applied in mechanical part retrieval scenarios, ensuring the engineering practicality of the comparison.

##### 3.2.2 Design of ablation experiments

To verify the effectiveness of the core modules of the proposed method, three control groups are set up, with only a single variable changed for each group:

Control Group 1: No weight optimization ( $w_l = w_\theta = w_c = w_r = 1/4$ );

Control Group 2: No special scenario deduction (protrusion/groove/length consistency);

Control Group 3: No diameter consistency constraint.

##### 3.2.3 Verification parameters and evaluation criteria

**Retrieval Parameters:** All methods are set to return the Top-10 results ( $K=10$ ). Since the median number of reference similar parts for the query parts is 9,  $K=10$  can cover most valid similar parts.

**Evaluation Criteria:** To comprehensively evaluate the performance of the bushing part retrieval method, an evaluation system is constructed from three dimensions—"precision, ranking quality, and efficiency"—covering the "validity, rationality, and practicality" of retrieval results.

### 3.3 Algorithm Verification Results and Performance Analysis

#### 3.3.1 Verification results of accuracy metrics

Accuracy metrics focus on the "purity" and "coverage" of retrieval results. The core metrics include Precision@K, Recall@K, and F1-score@K[16], with K set to 10 in this study.

**Table 2. Results of Accuracy Metrics**

Method	Precision@10	Recall@10	F1-score@10	Performance Improvement
CADF3D V4.2	0.3100	0.2867	0.2917	-
Control Group 3	0.5100	0.4733	0.4842	+66.0%
Control Group 2	0.7350	0.6800	0.7003	+140.1%
Control Group 1	0.8000	0.7133	0.7489	+156.7%
Proposed Method	0.8450	0.7867	0.8097	+177.6%

As indicated by the results:

CADF3D V4.2 exhibits insufficient precision and limited recall in part similarity matching, and its overall matching performance fails to meet the query quality requirements in practical application scenarios.

The three core metrics of the proposed method are significantly superior to those of the comparison method. The average F1-score@10 reaches 80.97%, which is a 177.6% improvement compared to CADF3D. This verifies the effectiveness of the technical route combining sketch profile encoding, bidirectional angle mapping, and sliding window matching.

Comparing the results of the ablation experiment groups, the performance ranking follows the order: "Proposed Method > Control Group 1 > Control Group 2 > Control Group 3 > CADF3D". This demonstrates that the three modules—weight optimization, sketch preprocessing, and path constraint—all contribute positively to performance.

#### 3.3.2 Verification results of ranking quality metrics

Ranking quality metrics evaluate the "orderliness" of retrieval results, with the core metric being Mean Average Precision (MAP@K) [17]. Similarly, the metric results of the 20 query parts were statistically summarized, and the performance improvement is defined as the increase relative to the minimum MAP@10 value. The results are presented in Table 3:

**Table 3. Results of Ranking Quality Metrics**

Method	MAP@10	Performance Improvement
CADF3D V4.2	0.2445	-
Control Group 3	0.3986	62.99%
Control Group 2	0.7445	204.50%
Control Group 1	0.8175	234.35%
Proposed Method	0.8799	259.88%

The metric results of the 20 query parts were statistically summarized, and the average Precision@10, Recall@10, and F1-score@10 of each method were calculated. The performance improvement is defined as the increase relative to the minimum F1 value. The results are shown in Table 2.

From the results: As the baseline method, CADF3D V4.2 achieves a MAP@10 of only 0.2445, which reflects the limitations of traditional methods in part similarity retrieval—specifically insufficient ranking quality and limited matching accuracy. By integrating core strategies including diameter constraints, special scenario deduction, and weight optimization, the full-version proposed method ultimately achieves a MAP@10 of 0.8799, representing a 259.88% improvement over the baseline method. Moreover, it outperforms all control groups in performance.

This further demonstrates that the optimized modules do not function in isolation; instead, they form an integrated solution with synergistic effects. This effectively addresses the core issues of traditional methods in part similarity retrieval, such as inadequate matching accuracy and flawed ranking logic.

**3.3.3 Verification results of efficiency metrics**  
 Efficiency metrics focus on the engineering practicality of the method, with the core metric being average response time. Retrieval was performed on all parts, followed by statistical analysis of retrieval durations to calculate the average time. The retrieval results are shown in Table 4[8], while Tables 5–7 provide detailed retrieval results for three different parts. This experiment compares the performance of CADF3D V4.2 and the proposed method from the perspective of time efficiency, objectively presenting the difference in retrieval time between the two methods for part similarity retrieval tasks: For CADF3D V4.2, the retrieval times of the three experiments are 1.93 s, 2.08 s, and 1.80 s, with an average of approximately 1.93 s. For the proposed method, the retrieval times of the three experiments are

7.646 s, 7.822 s, and 7.215 s, with an average of approximately 7.561 s. The retrieval time of the proposed method is significantly longer than that of the comparison method.

**Table 4. Retrieval Time Results**

Method	1st Experiment Time	2nd Experiment Time	3rd Experiment Time
CADFInd3D V4.2	1.93 s	2.08s	1.8 s
Proposed Method	7.646 s	7.822 s	7.215 s

**Table 5. Retrieval Results for Part 15DL-20000-01**

Query Model	Method	Retrieval Result				
	Proposed Method					
	CADFInd3D V4.2					

**Table 6. Retrieval Results for Part BYCQ63XF01-81**

Query Model	Method	Retrieval Result				
	Proposed Method					
	CADFInd3D V4.2					

**Table 7. Retrieval Results for Part DH2S8-82031PJ**

Query Model	Method	Retrieval Result				
	Proposed Method					
	CADFInd3D V4.2					

From the perspective of technical principles, the core reason for the longer time consumption of the proposed method lies in the following: To achieve high-precision part feature matching, the algorithm requires refined editing and parsing of the sketch feature tree of CAD parts. This process involves traversing the hierarchical structure of the feature tree, verifying the

correlation of feature parameters, and extracting core geometric topology information. Compared with CADFind3D V4.2, which directly calls a pre-set feature library for shallow matching, the proposed method adds computational steps for sketch feature tree editing and in-depth information extraction—an inherent cause of the additional time overhead.

It should be clarified that the longer time overhead is not meaningless performance loss, but a necessary technical cost to achieve breakthroughs in core matching accuracy. The editing and information extraction of the sketch feature tree can deeply mine the geometric feature details of parts, providing key data support for the significant improvement of core metrics such as MAP@10 and F1-score@10.

### 3.4 Result Analysis

In the retrieval of bushing parts, the proposed method demonstrates the optimal performance: its average F1-score@10 reaches 80.97%, representing a 177.6% increase compared to CADFind3D (an industrial commonly used plugin), and its MAP@10 rises by 259.88%. These differences are statistically significant, highlighting prominent engineering application value. However, the retrieval time still requires improvement.

All three core modules—weight optimization, special scenario deduction, and diameter constraint—effectively enhance retrieval performance. Among them, the diameter constraint is the most critical for avoiding extreme mismatches, with a contribution value of 40.2%.

### 4. Conclusions

To address the demand for accurate retrieval of bushing components, this study proposes a method based on SolidWorks sketch profiles. The core steps are as follows: The SolidWorks API is used to extract the core sketch associated with the rotational feature of bushing parts; A five-tuple feature is employed to capture the local structural details of bushings, enabling direct matching between design intent and 3D models; Bidirectional angle mapping and sliding window matching are adopted, and weights and similarity deductions for special scenarios are set according to the geometric characteristics of shaft-bushings.

This method solves key issues in 3D retrieval, such as reliance on sketch or view data and

format incompatibility. Experimental verification on 466 industrial-grade bushing parts shows that: compared to CADFind3D, the proposed method achieves a 177.6% increase in F1-score@10 and a 259.88% increase in MAP@10. It can be directly integrated into mechanical design workflows, providing an engineering solution for part reuse.

## References

- [1] Manda B, Bhaskare P, Muthuganapathy R. A convolutional neural network approach to the classification of engineering models. *IEEE Access*, 2021, 9:22711-22723.
- [2] Yang Z Y, Bai J, Li W J, et al. Triple hierarchical metric network for 3D model sketch retrieval. *Journal of Computer-Aided Design & Computer Graphics*, 2024, 36(11):1791-1804.
- [3] Han X F, Diao Z Y, Zhang C Y, et al. Single-view 3D model retrieval based on attention and view information. *Journal of Shandong University (Engineering Science)*, 2025, 55(04):48-55.
- [4] Zhou Y, Li W J, Ye D W, et al. Universal retrieval and classification algorithm for 3D models based on internal and external views. *Journal of Computer-Aided Design & Computer Graphics*, 1-12 [2025-12-06].
- [5] Zhu T. Research on 3D mechanical part model retrieval technology and software development based on PointNet neural network. Dalian Maritime University, 2024:1-57.
- [6] Ji H. Research on classification and retrieval method of 3D medical rehabilitation aids based on point cloud features. Sichuan University, 2024:1-65.
- [7] Cheng P. GNMR: 3D neuron geometric shape retrieval based on graph neural network. *Computer & Digital Engineering*, 2024, 52(04):1131-1136.
- [8] Fan H Y and Bo P B. 3D parametric tire pattern model retrieval based on geometric features. *Journal of Zhejiang University (Science Edition)*, 2023, 50(06):803-810+819.
- [9] Tai T Y. Research on video retrieval technology based on 3D convolutional neural network. North China University of Technology, 2024:1-59.
- [10] Zhang G Y and Shao H. Establishment of standard part library based on SolidWorks and VBA. *Development & Innovation of Machinery & Electrical Products*, 2025, 38(01):124-126.
- [11] Chang Q Q, Li M X, Zhou W H, et al. The Application of Tolerance Database in the Secondary Development of SolidWorks. *Applied Mechanics and Materials*, 2014, 3360(599-601):1910-1913.
- [12] Zhao X, He F, Li K, et al. Introducing an efficient method for feature extraction in image retrieval systems. *Scientific Reports*, 2025, 15(1):43664-43664.
- [13] Zhang K, Yu Y Y, Yang X H, et al. Exploration of ideological and political teaching practice in "Mechanical Drawing and CAD" based on craftsman training camp—Taking the teaching project "Mapping of Shaft-Bushing Parts" as an example. *Guangdong Vocational and Technical Education and Research*, 2024, (06):128-133.
- [14] Duchnowski R, Wyszkowska P. Laser scanning data processed using Mspli estimation and sliding window algorithm. *Reports on Geodesy and Geoinformatics*, 2025, 120(1):67-74.
- [15] Yang Y, Zhang P, Wang Y, et al. An attention-based parallel model with sliding window decomposition algorithm for water quality prediction. *Journal of Water Process Engineering*, 2025, 78:108751.
- [16] Xu A M, Da G X, Yu L, et al. Research on rail corrugation defect detection algorithm based on YOLOv8 and multi-dimensional feature enhancement module. *Modern Urban Transit*, 2025, (11):97-103.
- [17] Li D S, Wang G, Yu J, et al. Research on insulator defect detection algorithm based on YOLO11-PDL. *Intelligent Computer and Applications*, 1-12 [2025-12-07].